THE JOURNAL OF PHYSICAL CHEMISTRY A

Article

pubs.acs.org/JPCA

Dimers of Perhaloacetyl Cyanides: $CClF_2C(O)OC(CN)_2CClF_2$ and $CF_3C(O)OC(CN)_2CF_3$. Preparation, Properties, and Spectroscopy

Luis A. Ramos,[†] Sonia E. Ulic,[†] Rosana M. Romano,[†] Helmut Beckers,[‡] Helge Willner,[‡] Maofa Ge,[§] Shengrui Tong,[§] and Carlos O. Della Védova*[,†]

[†]CEQUINOR (UNLP-CONICET), Departamento de Química, Facultad de Ciencias Exactas, Universidad Nacional de La Plata, 47 esq. 115, 1900 La Plata, República Argentina

[‡]Fachbereich C - Anorganische Chemie, Bergische Universität Wuppertal, 42097 Wuppertal, Germany

[§]State Key Laboratory for Structural Chemistry of Unstable and Stable Species, Institute of Chemistry, Chinese Academy of Sciences, Beijing 100190, China

Supporting Information

ABSTRACT: The vapor of the new compound 1,1-dicyano-2-chloro-2,2-difluoroethyl chlorodifluoroacetate, $CClF_2C(O)OC(CN)_2CClF_2$ and of the known 1,1-dicyano-2,2,2-trifluoroethyl trifluoroacetate, $CF_3C(O)OC(CN)_2CF_3$, were investigated using vibrational spectroscopy tools. The existence of rotational isomerism was confirmed for $CClF_2C(O)OC(CN)_2CClF_2$ when the matrix isolated compound was examined in combination with the computational results applying quantum chemical models. From the four conformers *gauche-syn-gauche, gauche-syn-anti, syn-syn-anti, syn-syn-gauche* (the used nomenclature is with respect to the ϕ(ClC−C(O)), ϕ((O)C-OC), and ϕ(OC−CCl) torsion angles, respectively) predicted for $CClF_2C(O)OC(CN)_2CClF_2$ the first two forms can be evidenced using Ar-matrix IR spectroscopy, with the first one being the most abundant at room temperature. On the other side, the results obtained for $CF_3C(O)OC(CN)_2CF_3$ reveals the existence of only one *syn-syn-anti* form. $CClF_2C(O)OC(CN)_2CClF_2$ melts at −40 °C and its vapor pressure was fitted by the equation ln p = −4732.6 (1/*T*) + 10.75 (*p* [Atm], *T* [K]) in the range −20 to 20 °C. Its extrapolated boiling point is 167 °C. The first ionization potentials occur for $CClF_2C(O)OC(CN)_2CClF_2$ and $CF_3C(O)OC(CN)_2CF_3$ at 12.13 and 12.43 eV, respectively, and were attributed to the ejection of electrons formally located at the carbonylic oxygen lone-pair electrons (n_O). The proposed interpretation of the photoelectron spectrum is consistent with related molecules reported previously, and also with the prediction of Outer Valence Green's Functions (OVGF).

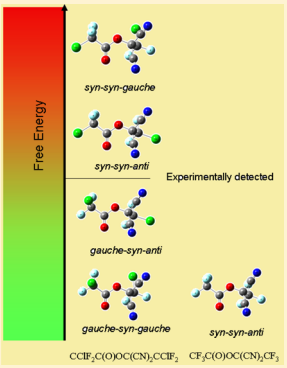

INTRODUCTION

The variation of the conditions in the preparation of chlorodifluoroacetyl cyanide can be readily used to form the dimer 1,1-dicyano-2-chloro-2,2-difluoroethyl chlorodifluoroacetate, $CClF_2C(O)OC(CN)_2CClF_2$. The related 1,1- dicyanoalquil carboxilato $CH_3C(O)OC(CN)_2CH_3$ has been used, for instance, to form the widely used vinylidene cyanide through the pyrolysis of the former compound.[1] In effect, during the synthesis of $CClF_2C(O)CN$[2] from $CClF_2C(O)Cl$ and AgCN a dimeric byproduct identified as $CClF_2C(O)OC(CN)_2CClF_2$ was formed.

$CClF_2C(O)OC(CN)_2CClF_2$ would be formed from $CClF_2C(O)CN$ with CN^- ions through an ionic species $CClF_2CO(CN)_2^-$ similar to cyanhidrine ($R_1R_2C(OH)C{\equiv}N$). Its further nucleophilic action on another $CClF_2C(O)CN$ yields $CClF_2C(O)OC(CN)_2CClF_2$ according to the following mechanism.

$CClF_2C(O)CN$ has been evidenced as an intermediate of the reaction since the product $CClF_2C(O)OC(CN)_2CClF_2$ can be also readily obtained using $CClF_2C(O)CN$ and AgCN as precursors. This mechanism has also been reported to explain the formation of $CH_3C(O)OC(CN)_2CH_3$.[3] The already known 1,1-dicyano-2,2,2-trifluoroethyl trifluoroacetate molecule,

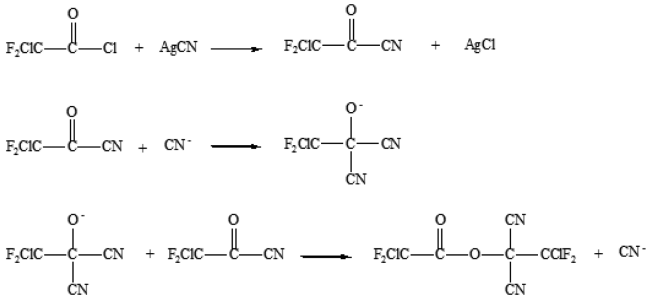

$CF_3C(O)OC(CN)_2CF_3$, formed from $CF_3C(O)Cl$ and AgCN,[4] has been also characterized in the present work. Very recently, benzoyl cyanide was reported to be ideally suited for quantitative, time-resolved analysis of RNA folding and ribonucleoprotein (RNP) assembly mechanisms.[5] This compound was used as a fast-acting reagent reacting either to form a 2′-O-adduct at conformationally flexible nucleotides or to undergo rapid self-inactivation by hydrolysis.[6] In view of these

Received: December 30, 2013
Revised: February 11, 2014
Published: February 17, 2014

   dx.doi.org/10.1021/jp4127732 | *J. Phys. Chem. A* 2014, 118, 1721−1729

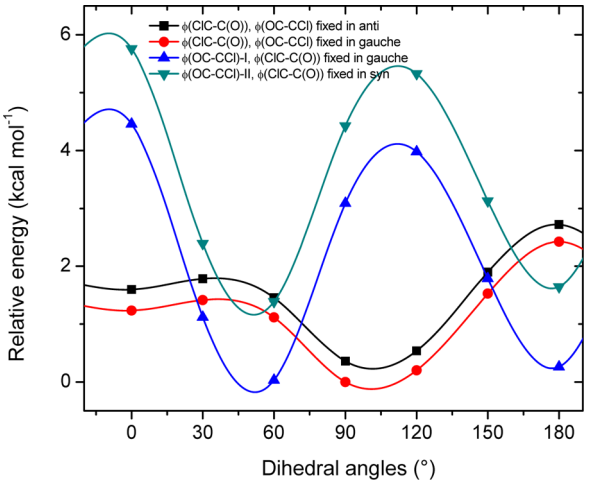

Figure 1. Calculated potential energy curves for the internal rotation in dependence of variations of ϕ(ClC−C(O)) (for ϕ(OC−CCl) in *gauche* (red) and *anti* (black)) and ϕ(OC−CCl) (for ϕ(ClC−C(O)) in *gauche* (blue) and *syn* (green)) dihedral angles of $CClF_2C(O)OC(CN)_2CClF_2$ by using the B3LYP/6-31G(d) method. The relax scan of the potential energy surface was performed by rotating the dihedral angles in steps of 30° while keeping the rest of the molecule optimized.

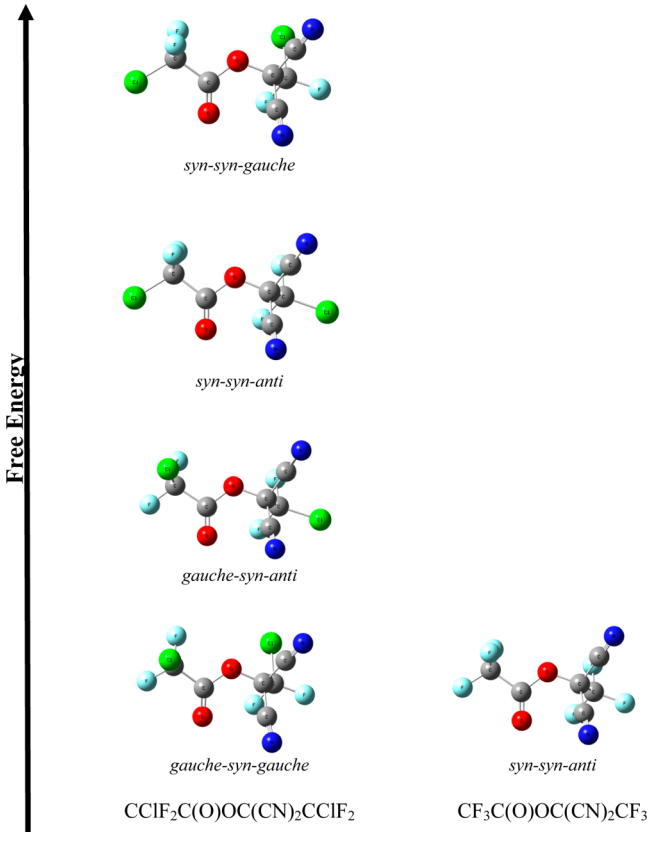

Figure 2. Optimized structures and relative energies of the most abundant conformers for $CClF_2C(O)OC(CN)_2CClF_2$ and $CF_3C(O)OC(CN)_2CF_3$ computed with the method B3LYP/6-311+G(d).

antecedents, we report herein the first synthesis of 1,1-dicyano-2-chloro-2,2-difluoroethyl chlorodifluoroacetate, $CClF_2C(O)OC(CN)_2CClF_2$.

The physical (vapor pressure vs temperature behavior) and spectroscopic properties (NMR, UV) including photoelectron spectroscopy (PES) have been studied. The conformational properties of this compound were investigated using vibrational spectroscopy (IR matrix, Raman) as guided by quantum chemical calculations. The reported but not deeply characterized 1,1-dicyano-2,2,2-trifluoroethyl trifluoroacetate, $CF_3C(O)OC(CN)_2CF_3$, has been also included in the present study with the sake of comparison.

Table 1. Calculated Relative Total Energies ($\Delta E°$, kcal mol^{-1}), Standard Gibbs Free Energy Differences ($\Delta G°$, kcal mol^{-1}), and Boltzmann Predicted Distributions in the Gas Phase for the Four Conformers of $CClF_2C(O)OC(CN)_2CClF_2$ Computed with the Model B3LYP/6-311+G(d)[a]

conformer	$\Delta E°$	$\Delta G°$	(%)
gauche-syn-gauche	0.13	0.00	57
gauche-syn-anti	0.00	$2.5.10^{-3}$	29
syn-syn-anti	1.19	0.28	9
syn-syn-gauche	1.33	1.03	5

[a]The values are relative with respect to the more stable *gauche-syn-gauche* form. Degeneracies of the forms are taken into account.

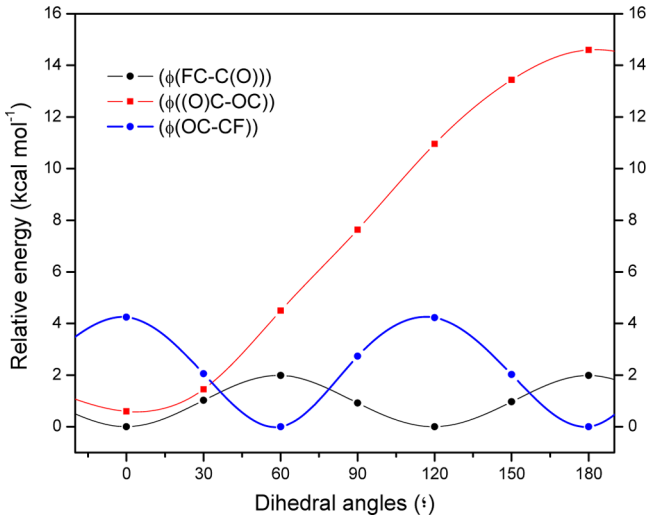

Figure 3. Calculated potential energy curves for the internal rotation in dependence of variations of ϕ(FC−C(O)) (black), ϕ((O)C-OC) (red), and ϕ(OC−CF) (blue) dihedral angles of $CF_3C(O)OC(CN)_2CF_3$ by using the B3LYP/6-31G(d) method. The relax scan of the potential energy surface was performed by rotating the dihedral angles in steps of 30° while keeping optimizing the rest of the molecule.

Instrumentation and Procedure. *(a). General Procedure.* Volatile materials were manipulated in a glass vacuum line equipped with a capacitance pressure gauge (221 AHS-1000, MKS Baratron, Burlington, MA), three U-traps and valves. The pure compounds were stored in flame-sealed glass ampules under liquid nitrogen in a Dewar vessel. The ampules were opened with an ampule key at the vacuum line, an appropriate amount was taken out for the experiments, and then they were flame-sealed again.[7] The vapor pressures of the samples were measured in a small vacuum line equipped with a calibrated capacitance pressure gauge (MKS Baratron, AHS-100) and a small sample reservoir. Both dimer compounds are liquid at ambient temperature.

(b). Vibrational Spectroscopy. Infrared gas spectra were recorded on a Bruker Vector 25 spectrometer and on a Bruker EQUINOX 55 FTIR spectrometer, with a resolution of 2 cm^{-1} in the range from 4000 to 400 cm^{-1}.

dx.doi.org/10.1021/jp4127732 | J. Phys. Chem. A 2014, 118, 1721−1729

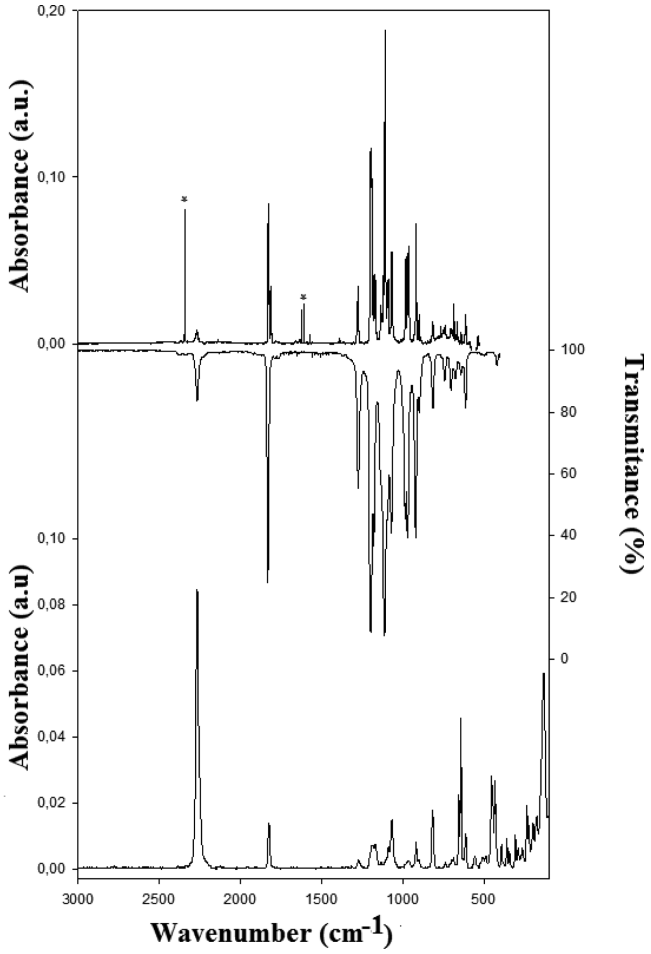

Figure 4. Upper trace: IR spectrum of $CClF_2C(O)OC(CN)_2CClF_2$ isolated in solid Ar (1:2000) at 15 K (resolution: 0.25 cm^{-1}). Middle trace: IR spectrum of gaseous $CClF_2C(O)OC(CN)_2CClF_2$ at 298 K (resolution: 2 cm^{-1}). Lower trace: Raman spectrum of liquid $CClF_2C(O)OC(CN)_2CClF_2$ at 298 K (resolution: 2 cm^{-1}). *Signals corresponding to CO_2 and H_2O.

Raman spectra of neat liquids were measured at room temperature in flame-sealed capillaries (3 mm o.d.) on a FT Bruker RFS 106/S spectrometer, equipped with a 1064 nm Nd:YAG laser, in the region from 4000 to 100 cm^{-1} using a resolution of 2 cm^{-1}.

(c). Matrix Isolation Experiments. Matrix isolation experiments were carried out diluting $CClF_2C(O)OC(CN)_2CClF_2$ with argon in a ratio of 1:1000 in a 1 L stainless-steel storage container, and then small amounts of the mixture were deposited within 10 min onto the cold matrix support (16 K, Rh-plated Cu-block) in a high vacuum (10^{-5} Pa). IR spectra of matrix-isolated samples were recorded in a reflectance mode on a Bruker IFS 66v/S spectrometer using a transfer optic. A liquid N_2 cooled HgCdTe detector (MCT) and a KBr/Ge beam splitter were used in the wavenumber range 5000 to 530 cm^{-1}. For each spectrum with an apodized resolution of 0.25 cm^{-1}, 200 scans were added. More details of the matrix apparatus are given elsewhere.[8]

(d). UV Spectroscopy. The UV−visible spectra of the gaseous samples were recorded using a glass cell equipped with quartz windows (10 cm optical path length) on a Lambda EZ210 UV/vis spectrometer (Perkin-Elmer). Measurements were carried out in the spectral region from 190 to 500 nm with a sampling interval of 1.0 nm, a scan speed of 200 nm min^{-1}, and a slit of 2 nm.

(e). NMR Spectroscopy. For ^{13}C and ^{19}F NMR spectra, pure samples were flame-sealed in thin-walled 4 mm o.d. tubes and placed into 5 mm NMR tubes. The NMR spectra were recorded on a Bruker Avance 400 spectrometer at 100.6 and 376.5 MHz, respectively. The samples of $CClF_2C(O)OC(CN)_2CClF_2$ and $CF_3C(O)OC(CN)_2CF_3$ were held at 25 °C and C_6D_6 or CD_2Cl_2, respectively, were used as an external lock and reference.

(e). Quantum Chemical Calculations. DFT calculations were performed using the program package GAUSSIAN 03.[9] In all cases, not scaled frequencies will be reported.

Synthesis. Both $CClF_2C(O)OC(CN)_2CClF_2$ and $CF_3C(O)OC(CN)_2CF_3$ were synthesized by treatment of the corresponding $CClF_2C(O)Cl$ or $CF_3C(O)Cl$ with an excess of silver cyanide and subsequently characterized vibrationally. For the preparation of $CClF_2C(O)OC(CN)_2CClF_2$, 1.0 g of $CClF_2C(O)Cl$ was distilled onto 1.3 g of dry AgCN in a 250 mL glass vessel provided with a Young valve with PTFE stems (Young, London, U.K.). The reaction was carried out in vacuum for 2 h at 50 °C. Purification of the product was performed by trap-to-trap distillations with traps held at −52, −95, and −196 °C. $CClF_2C(O)OC(CN)_2CClF_2$ was mainly isolated in the trap at −52 °C. The final yield was 75%.

The same scheme was used to prepare $CF_3C(O)OC(CN)_2CF_3$. In this case, 1.0 g of $CF_3C(O)Cl$ and 1.4 g of AgCN were used. The reaction was carried out in vacuum for 15 h at 80 °C. The selected temperatures for the traps were −70, −100, and −196 °C. $CF_3C(O)OC(CN)_2CF_3$ was isolated mainly in the first trap with a final yield of 10%.

General Properties. Solid 1,1-dicyano-2-chloro-2,2-difluoroethyl chlorodifluoroacetate, $CClF_2C(O)OC(CN)_2CClF_2$ melts at −40 °C to a colorless liquid. Its vapor pressure was recorded in the −20 to 20 °C range and is fitted with the equation $\ln p = -4732.6\,(1/T) + 10.75$ (p [atm], T [K]), being 167 °C its extrapolated boiling point. The analogous 1,1-dicyano-2,2,2-trifluoroethyl trifluoroacetate, $CF_3C(O)OC(CN)_2CF_3$, melts at −21 °C and its vapor pressure can be fitted by the expression $\ln p = -4808.6\,(1/T) + 13.57$ (p [atm], T [K]) in the −18 to 22 °C range. Its extrapolated boiling point of 81 °C is lower than the corresponding value extrapolated for $CClF_2C(O)OC(CN)_2CClF_2$ in agreement with an increase of the volatility by formal substitution of a Cl by a F atom in $CClF_2C(O)OC(CN)_2CClF_2$. Both compounds are stable at room temperature.

The ^{19}F NMR spectrum of the $CClF_2C(O)OC(CN)_2CClF_2$ liquid shows two singlets at $\delta = -64.2$ and −64.9 ppm attributed to the fluorine atoms of the $CClF_2$ groups; the ^{13}C NMR spectrum exhibits four triplet signals centered at 155.0 ppm ($^2J_{(C-F)}$ = 39.5 Hz), 122.4 ppm ($^1J_{(C-F)}$ = 302.98 Hz), 115.8 ppm ($^1J_{(C-F)}$ = 300.4 Hz) and 66.8 ppm ($^2J_{(C-F)}$ = 36.6 Hz), and one singlet signal at 105.9 ppm. They were concomitantly assigned to the carbon atoms of the C═O, $CClF_2$ (bonded to the C═O), $CClF_2$ (bonded to the quaternary carbon), the quaternary C and CN, respectively. (Figure S1, Supporting Information). The chemical shifts are close to those reported for similar compounds.[2,10,11]

A similar behavior was found in the case of $CF_3C(O)OC(CN)_2CF_3$. Its ^{19}F NMR spectrum shows two singlet at $\delta = -73.8$ and −75.5 ppm assigned to both CF_3 groups; the ^{13}C NMR spectrum exhibits four quartet signals centered at 153.6 ppm ($^2J_{(C-F)}$ = 49.0 Hz), 118.6 ppm ($^1J_{(C-F)}$ = 289.1 Hz), 113.8 ppm ($^1J_{(C-F)}$ = 285.8 Hz), and 62.6 ppm ($^2J_{(C-F)}$ = 41.3 Hz), and one singlet signal at 105.30 ppm. They were assigned to carbon atoms of the C═O, CF_3 (bonded to C═O), CF_3 (bonded to the quaternary carbon), the quaternary carbon and the CN, respectively. (Figure S2, Supporting Information).

dx.doi.org/10.1021/jp4127732 | J. Phys. Chem. A 2014, 118, 1721−1729

Table 2. Experimental and Calculated Frequencies (cm^{-1}) and Assignments of the Fundamental Vibrational Modes of $CClF_2C(O)OC(CN)_2CClF_2$

	experimental				computed conformations[a]		
mode	IR (gas)[b]	IR (Ar matrix)[c]	Raman (liquid)[d]		*gauche-syn-gauche*	*gauche-syn-anti*	assignment[e]
ν_1	2266 w	2267.3	2267	100	2376 (7)	2377 (8)	ν(C4N)
ν_2		2257.1	2254		2365 (9)	2368 (9)	ν(C5N)
ν_3	1831 s	1827.3*/1822.6/1813.4/1809.9	1824	16	1881 (235)	1881 (234)	ν(C═O)
ν_4	1275 m	1279.9/1279.5	1275/1268	3	1250 (98)	1249 (98)	ν(C1−C2), ν(C2−O)
ν_5	1198 vs	1198.2/1192.1	1189	9	1182 (222)	1185 (104)	$\nu_{as}(C1ClF_2)$, $\nu_{as}(C6ClF_2)$ in phase
ν_6	1179 sh, m	1176.2	1169	9	1166 (137)	1169 (268)	$\nu_{as}(C1ClF_2)$, $\nu_{as}(C6ClF_2)$ out of phase
ν_7	1133 sh, m 1113 vs	1136.1 1109.5	1135	3	1147 (178)	1161 (188)	ν(C3−C6)
ν_8					1141 (164)	1129 (223)	$\nu_{as}(C6ClF_2)$
ν_9	1093 sh, m	1089.5	1087	8	1095 (364)	1094 (393)	ν(C2−O), $\nu_s(C1ClF_2)$
ν_{10}	1071 m	1069.3*/1064.7	1068	18	1067 (114)	1050 (72)	ν(C3−O)
ν_{11}	985 m	982.4	976	3	1024 (115)	1022 (48)	ν(C3−C6), ν_s(C3−O)
ν_{12}	970 m	965.2	964	3	949 (234)	955 (341)	$\nu_s(C1ClF_2)$, ν(C(O)-O)
ν_{13}	921 m	919.7	919	10	886 (154)	897 (72)	$\nu_s(C6ClF_2)$
	898 sh, w	901.1/899.1	903	4			
ν_{14}	815 w	818.5/813.4	818	21	832 (50)	833 (64)	δ(O═C−O)
ν_{15}	741 vw	740.3	739	3	730 (16)	722 (28)	δ(C1C2(O)O)
ν_{16}	702 vw 676 vw	705.6 676.4	700 687	4 4	701 (50)	681 (57)	$\delta(C3-C4-C5)_{wag}$, δ(C1C2(O)O)
ν_{17}	- 642 vw	- 642.5	655 643	28 58	639 (12)	651 (4)	$\delta(C6F_2)$
ν_{18}	614 vw	615.9	614	13	611 (19)	611 (23)	$\delta(C1F_2)$
ν_{19}			557	5	581 (1)	581 (1)	$\delta(C3-C4-C5)_{sci}$
ν_{20}			508	4	507 (4)	520 (<1)	$\delta(C3-C4-C5)_{twist}$
ν_{21}			488	4	497 (2)	502 (4)	ρ(C3−C4−C5)
ν_{22}			455	34	467 (3)	462 (2)	ρ(C3−C4−C5)
ν_{23}			448	30	442 (1)	437 (1)	ν(C6−Cl), $\delta(C6F_2)$
ν_{24}			433	33	428 (1)	427 (2)	ν(C1−Cl), $\delta(C1F_2)$
ν_{25}			419 h	6	419 (<1)	386 (<1)	ρ(C3C4C5), ν(C1−Cl), $\delta(C1F_2)$
ν_{26}			392	9	388 (12)	417 (5)	ρ(C3C4C5), $\rho(C6ClF_2)$
ν_{27}			382	1	355 (1)	359 (3)	δ(C1C2(O)O)
ν_{28}			359	11	351 (4)	345 (13)	$\rho(C6ClF_2)$
ν_{29}			308	13	311 (6)	317 (3)	$\rho(C1ClF_2)$
ν_{30}			290	8	301 (1)	301 (5)	ρ(C3C4C5)
ν_{31}			263	8	253 (1)	273 (8)	-
ν_{32}			236	23	238 (9)	217 (1)	δ(C2−O−C3)
ν_{33}			198	16	188 (<1)	191 (<1)	δ(Cl−C6−C3)
ν_{34}			174	19	162 (3)	158 (2)	δ(Cl−C1−C2)
ν_{35}			133	69	144 (3)	145 (3)	-
ν_{36}					126 (2)	130 (1)	-
ν_{37}					119 (3)	119 (5)	-
ν_{38}			99	20	98 (2)	100 (2)	δ(C1−C2−O)
ν_{39}					79 (<1)	85 (<1)	τ((O)C2−OC3)
ν_{40}					42 (<1)	47 (<1)	$\tau(C6ClF_2-C3C5)$
ν_{41}					37 (<1)	38 (<1)	$\tau(C1ClF_2-C(O))$
ν_{42}					22 (<1)	23 (<1)	τ(C1C2−OC3)

[a]B3LYP/6-311+G(d) calculated frequencies (cm^{-1}). IR intensities are given between parentheses (km mol^{-1}). [b]Relative band intensities: vs; very strong, s, strong; m, medium; w, weak; vw, very weak. [c]The most intense Ar-matrix site is indicated with the star. [d]Relative intensities based on the integration of band areas are given in the parentheses. [e]The number of the atoms are $C1ClF_2C2(O)OC3(C4N)(C5N)C6ClF_2$. ν, δ, ρ and τ represent stretching, deformation, rocking and torsion modes, respectively.

The UV−vis spectrum of gaseous $CClF_2C(O)OC(CN)_2CClF_2$ and $CF_3C(O)OC(CN)_2CF_3$ (Figure S3) are very similar. They show one absorption band with λ_{max} = 219 and 217 nm, respectively. These features are assigned to a $n \rightarrow \pi^*$ transition.[8] Figure S3 also includes the UV−vis spectrum of $CClF_2C(O)CN$ for comparison.[2]

RESULTS AND DISCUSSION

Calculated Conformers and Relative Energies. The conformational properties of $CClF_2C(O)OC(CN)_2CClF_2$ were explored by locating the minimum energy structures on the potential energy curves around the ϕ(ClC−C(O)) and ϕ(OC−CCl) dihedral angles by using the approximation B3LYP/6-31G(d) (Figure 1) since only one minimum has been computed for the (O)C−OC torsional angle. These curves have been obtained relaxing the ϕ(ClC−C(O) torsional angle and fixing ϕ(OC−CCl) in *gauche* (red) or *anti* (black) and relaxing the ϕ(OC−CCl) torsional angle and fixing ϕ(ClC−C(O)) in *gauche* (blue) or *syn* (green). Thus, four low-energy conformers,

dx.doi.org/10.1021/jp4127732 | J. Phys. Chem. A 2014, 118, 1721−1729

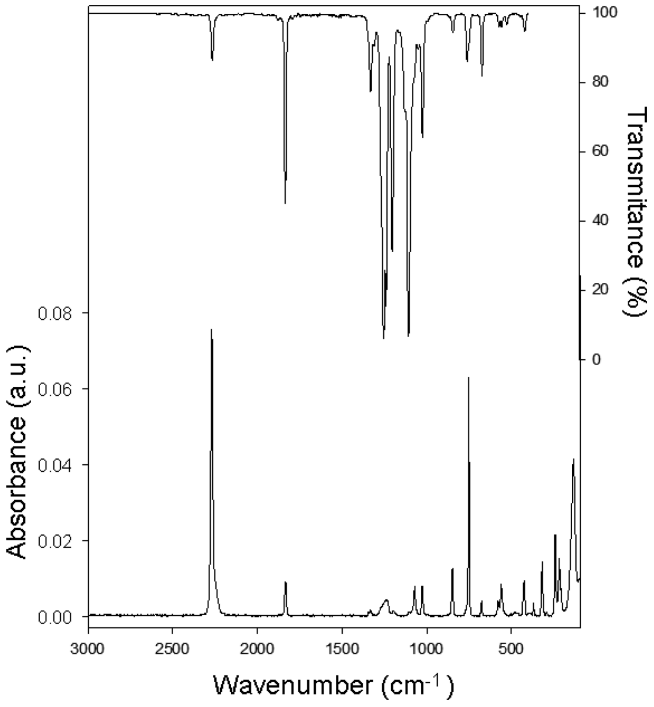

Figure 5. Upper trace: IR spectrum of gaseous $CF_3C(O)OC(CN)_2CF_3$ at 298 K (resolution: 2 cm^{-1}). Lower trace: Raman spectrum of liquid $CF_3C(O)OC(CN)_2CF_3$ at 298 K (resolution: 2 cm^{-1}).

gauche-syn-gauche, *gauche-syn-anti*, *syn-syn-anti*, and *syn-syn-gauche*, were found on the potential energy surface as depicted in the Figure 2. Table 1 lists the energy differences computed with the B3LYP/6-311+G(d) method for these forms of $CClF_2C(O)OC(CN)_2CClF_2$. According to this approximation, the form *gauche-syn-gauche* represents the most abundant conformation with an abundance of 57% followed by the *gauche-syn-anti* (29%), *syn-syn-anti* (9%), and *syn-syn-gauche* (5%) forms.

The formal substitution of a $CClF_2$ in $ClF_2C(O)OC(CN)_2CClF_2$ by a symmetric CF_3 group to give $CF_3C(O)OC(CN)_2CF_3$ simplifies the case (Figure 3). $CF_3C(O)OC(CN)_2CF_3$ is present in only one *syn-syn-anti* conformation (see also the Figure 2).

Vibrational Spectra. *$CClF_2C(O)OC(CN)_2CClF_2$.* IR spectra of $CClF_2C(O)OC(CN)_2CClF_2$ (gas-phase and Ar-matrix) and the Raman spectrum of the liquid were recorded, the results are shown in Figure 4. The observed band positions are listed in Table 2 and compared with the calculated frequencies for the two lowest energy conformers.

Beside the use of the computed frequency trend, the assignment of the normal modes of vibration of $CClF_2C(O)OC(CN)_2CClF_2$ was performed by comparison with results reported in the literature for similar molecules as $CF_3C(O)CN$,[4] $FC(O)CN$,[12] $CF_2ClC(O)NCO$,[13] $CClF_2C(O)NCS$,[14] and $CClF_2C(O)N_3$.[15] Its $3N - 6 = 42$ normal modes of vibration are all IR and Raman active for each form.

According to the theoretical calculations (Table 1), the global minimum *gauche-syn-gauche* is expected to be in equilibrium with the *gauche-syn-anti* form at ambient temperature with a remainder minor composition of the *syn-syn-gauche* and *syn-syn-anti* rotamers. However, the analysis of the vibrational spectra assignments is limited to the two most abundant forms since no experimental evidence have been found for the two less abundant rotamers. Differences between the computed frequencies of both *gauche-syn-gauche* and *gauche-syn-anti* forms give a special insight for the conformational assignment listed in Table 2.

Matrix-isolation IR spectroscopy is an important tool for studying conformational equilibria.[16] The IR fundamentals of Ar-matrix-isolated $CClF_2C(O)OC(CN)_2CClF_2$ (1:2000) show weak satellite bands within a few wavenumbers, which are attributed in part to the presence of the conformers, as evidenced by the proximity between the experimental and calculated $\Delta\nu$ in Table 2.

The most remarkable insights are evidenced in the regions of 700 and 650 cm^{-1}, respectively, where band splits become apparent.

The antisymmetric and symmetric stretching modes of the CN groups were observed at 2266 cm^{-1} and 2267 in the gas infrared and in the liquid Raman spectra, respectively. In the matrix IR spectrum two bands appeared at 2267.3 and 2257.1 cm^{-1}. The gas IR band at 1831 cm^{-1} and liquid Raman band at 1824 cm^{-1} are assigned to the ν(C═O) fundamental in comparison with reported data for similar molecules, such as $CF_3C(O)NCO$ (1795 and 1785 cm^{-1})[17] and $ClF_2CC(O)N_3$ (1759 cm^{-1}).[15] This higher C═O frequency for $CClF_2C(O)OC(CN)_2CClF_2$ can be rationalized taking into account that the C═O vibration depends on the sum of the electronegativities attached to the C═O double bond.[18] The C═O bond is linked to a $CClF_2$ group and to a neighbor O atom belonging to the $OC(CN)_2CClF_2$ fragment of $CClF_2C(O)OC(CN)_2CClF_2$.

The C−F and C−C stretching regions show bands at 1275 cm^{-1} and 1133 cm^{-1} in the gas IR spectrum assigned to the $CClF_2C$−C(O) group (coupled with (O)C−O) and OC−$CClF_2$ vibrational modes), respectively. Observed bands at 1198 and 1179 cm^{-1} in the gas IR are assigned to the $CClF_2$ stretching vibrations and the intense feature at 1113 cm^{-1} belong to a coupled mode formed with $\nu_s(CClF_2)$ and (O)C−O stretching.

Weak Raman bands observed at 700 and 687 cm^{-1} can be assigned to C3−C4−C5 waging mode coupled with the C1C2(O)O deformation of the two main conformers in agreement with the $\Delta\nu$ of 10 cm^{-1} predicted for these forms (B3LYP/6-311+G(d)).

A very weak band at 642 cm^{-1} is assigned to the CF_2 deformation mode. Its computed $\Delta\nu$ of 12 cm^{-1} for the two main rotamers (B3LYP/6-311+G(d)) agrees exactly with the difference observed in this region for the two liquid Raman bands at 655 and 643 cm^{-1}, respectively, giving additional confidence to the existence of two rotamers in equilibrium at ambient temperature.

Due to the coupled normal modes of vibration the assignment proposed in Table 2 is only approximate for $CClF_2C(O)OC(CN)_2CClF_2$.

$CF_3C(O)OC(CN)_2CF_3$. Vibrational spectra of $CF_3C(O)OC(CN)_2CF_3$ are depicted in the Figure 5 and listed in Table 3

The computed values calculated with the model B3LYP/6-311+G(d) predict only one stable *syn-syn-anti* conformation and its $3N - 6 = 42$ modes are expected to be IR and Raman active. Moreover, the simplicity of both gas IR and liquid Raman spectra supports the existence of only one conformation for the molecule. Furthermore, the spectra are similar to $CClF_2C(O)OC(CN)_2CClF_2$. Thus, the assignment was made by comparison with this species.

The characteristic bands at 2268 cm^{-1} and 1838 cm^{-1} in the gas IR spectrum can be assigned to the C≡N and C═O stretching vibrations, respectively. The liquid Raman counterpart of the former vibration in the Raman spectrum at 2270 cm^{-1} is the most intense band as in the case of $CClF_2C(O)OC(CN)_2CClF_2$.

dx.doi.org/10.1021/jp4127732 | J. Phys. Chem. A 2014, 118, 1721−1729

Table 3. Experimental and Calculated Frequencies (cm^{-1}) and Assignments of the Fundamental Vibrational Modes of $CF_3C(O)OC(CN)_2CF_3$

	experimental			computed conformation[a]	
mode	IR (Gas)[b]	Raman (liquid)[c]		*syn-syn-anti*	assignment[d]
ν_1	2268 w	2270	100	2377 (7)	ν(C4N)
ν_2				2368 (10)	ν(C5N)
ν_3	1838 m	1834	13	1888 (238)	ν(C═O)
ν_4	1334 w	1334	3	1300 (56)	ν(C1−C2), ν(C2−O)
ν_5	1257 vs	1260	4	1228 (417)	$\nu_{as}(ClF_3)$, $\nu_{as}(C6F_3)_{in\ phase}$
ν_6	1243 s	1235	6	1219 (250)	$\nu_{as}(C6F_3)$
ν_7	1207 m	1197	1	1214 (64)	$\nu_{as}(ClF_3)$, $\nu_{as}(C6F_3)_{out\ of\ phase}$
ν_8				1200 (175)	$\nu_{as}(C6F_3)$
ν_9	1134 w			1162 (285)	$\nu_{as}(C1F_3)$
ν_{10}				1143 (206)	ν_{as}(C4C3C5)
ν_{11}	1110 vs	1105	1	1091 (578)	ν(C2−O), $\nu_s(C1F_3)$
ν_{12}	1074 w	1072	10	1053 (62)	ν(C3−O)
ν_{13}	1029 w	1027	10	983 (60)	ν(C3−C6)
ν_{14}	848 vw	849	17	855 (20)	δ(O═C−O) $\nu_s(C1F_3)$
ν_{15}	764 w			764 (15)	δ(C1C2(O)O)
ν_{16}	755 w	753	93	758 (20)	$\delta(C1F_3)$, $\delta(C6F_3)_{our\ of\ phase}$
ν_{17}				737 (14)	$\delta(C1F_3)$, $\delta(C6F_3)_{in\ phase}$
ν_{18}	677 w	677	6	681 (25)	$\delta(C3(C4C5))_{wag}$
ν_{19}	575 vw	580	6	581 (1)	$\delta(C3(C4C5))_{sci}$
ν_{20}				571 (1)	$\delta(C3(C4C5))_{twist}$, $\delta_{as}(C1F_3)$
ν_{21}	560 vw	561	11	564 (1)	$\delta_s(C1F_3)$, $\delta_s(C6F_3)$
ν_{22}				556 (5)	$\delta_{as}(C1F_3)$, $\delta(C6F_3)$, $\delta(C3(C4C5))_{sci}$
ν_{23}	530 vw			517 (6)	$\delta_{as}(C1F_3)$
ν_{24}				483 (2)	$\delta(C3(C4C5))_{twist}$
ν_{25}				455 (1)	ρ(C3(C4C5))
ν_{26}	425 vw	426	11	425 (8)	-
ν_{27}				407 (2)	ρ(C3(C4C5)), δ(C1C2(O)O), $\delta_s(C1F_3)$
ν_{28}		371	6	393 (6)	$\rho(C6F_3)$
ν_{29}		320	13	328 (4)	ρ(C3(C4C5)), $\rho(C1F_3)$
ν_{30}				318 (1)	$\rho(C1F_3)$
ν_{31}		291	1	289 (5)	$\rho(C1F_3)$
ν_{32}		243	29	241 (10)	δ(C2−O−C3)
ν_{33}		219	21	210 (<1)	-
ν_{34}		209	10	194 (2)	δ(C1−C2−O)
ν_{35}		135	54	144 (3)	-
ν_{36}				130 (2)	-
ν_{37}				123 (4)	-
ν_{38}				102 (2)	-
ν_{39}				79 (<1)	τ((O)C−OC3)
ν_{40}				48 (<1)	$\tau(C6F_3-C3C5)$
ν_{41}				42 (<1)	$\tau(C1F_3-C(O))$
ν_{42}				30 (<1)	τ(C1C2−OC3)

[a]B3LYP/6-311+G(d) calculated frequencies (cm^{-1}). IR intensities are given between parentheses (km mol^{-1}). [b]Relative band intensities: vs; very strong, s, strong; m, medium; w, weak; vw, very weak. [c]Relative intensities based on the integration of band areas are given in the parentheses. [d]The number of the atoms are $C1F_3C2(O)OC3(C4N)(C5N)C6F_3$. ν, δ, ρ, and τ represent stretching, deformation, rocking and torsion modes, respectively.

Stretching vibrations corresponding to the ester group are observed at 1110 and 1074 cm^{-1} and were assigned to the (O)C−O and O−$C(CN)_2$ modes, respectively. CF_3 stretching vibrations are also observed in the expected region being very intense and weak bands in gas infrared and liquid Raman spectra, respectively.

Photoelectron Spectra. *$CClF_2C(O)OC(CN)_2CClF_2$*. Photoelectron spectroscopy (PES) using a He(I) radiation (21.21 eV = 58.46 nm) is an useful technique to study the valence electronic structure of molecules in combination with theoretical calculations.[19−21] The He(I) photoelectron spectrum of $CClF_2C(O)OC(CN)_2CClF_2$ is shown in Figure 6. Outer Valence Green Function (OVGF) calculations were performed to obtain the ionization energies in order to assign the PE spectrum. The experimental vertical ionization potentials (IP), theoretical vertical ionization energies (E_v; OVGF/6-311+G(d)), molecular orbitals (MO), and the corresponding characters of outer valence shells for $CClF_2C(O)OC(CN)_2CClF_2$ are listed in Table 4.

Additionally, the representation of the first 12 HOMOs is given in Figure S4 (Supporting Information). In agreement with the above discussion on the structure of $CClF_2C(O)OC(CN)_2CClF_2$, its He(I) photoelectron spectrum is the result of

dx.doi.org/10.1021/jp4127732 | J. Phys. Chem. A 2014, 118, 1721−1729

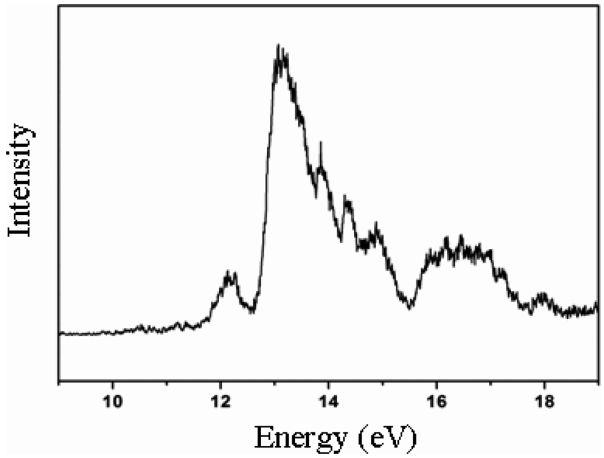

Figure 6. He(I) photoelectron spectrum (PES) of $CClF_2C(O)OC(CN)_2CClF_2$.

Table 4. Experimental and Calculated Ionization Energies and MO Characters for $CClF_2C(O)OC(CN)_2CClF_2$

band	EI exp. (eV)	E_v calc.[a] (eV)	MO	character
1	12.13	12.57	68	n_O
2	12.27	12.89	67	$n_{Cl\ (CClF2C(O))}$
3	13.09	13.22	66	$n_{Cl\ (CClF2C(O))}$
		13.21	65	$n_{Cl\ (C(CN)2\ CClF2)}$
4	13.84	13.57	64	$n_{Cl\ (C(CN)2\ CClF2)}$
		13.66	63	$n_{O\ (C(O))}$, $n_{O\ (OC)}$
5	14.33	14.13	62	π_{C1N1}, π_{C2N2}
		14.18	61	π_{C1N1}
6	14.74	14.60	60	π_{C2N2}
7	14.86	14.93	59	σ_{C1N1}, π_{C2N2}
		14.95	58	σ_{C1N1}, σ_{C2N2}
8	15.01	15.08	57	n_F

[a]OVGF from geometries at the B3LYP/6- 311+G(d) level of approximation for the *gauche-syn-gauche* form.

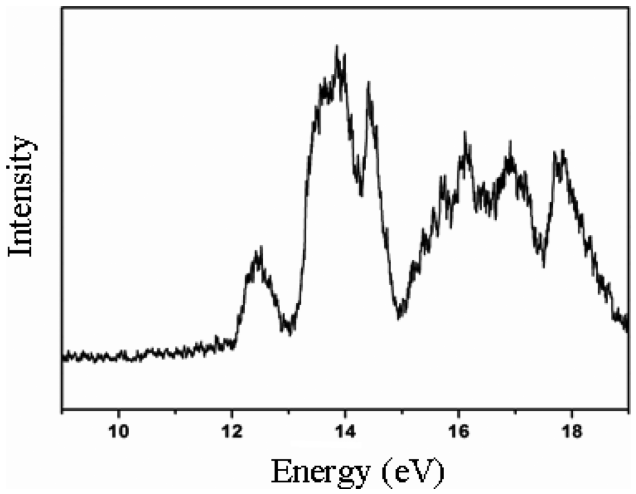

Figure 7. He(I) photoelectron spectrum (PES) of $CF_3C(O)OC(CN)_2CF_3$.

the weighted forms mainly arising from the energetically most favorable *gauche-syn-gauche* and *gauche-syn-anti* rotamers. In this respect, theoretical computations (OVGF/6-311+G(d)) for the two forms do not predict noticeable differences in the ionization energies with respect to the experimental resolution of 30 meV

Table 5. Experimental and Calculated Ionization Energies and MO Characters for $CF_3C(O)OC(CN)_2CF_3$

band	EI exp. (eV)	E_v calc.[a] (eV)	MO	character
1	12.43	12.97	60	$n_{O(C=O)}$
2	13.65	13.33	59	$n_{O(O-C)}$
		13.33	58	π_{C1N1}, π_{C2N2}
		13.70	57	π_{C1N1}, π_{C2N2}
3	13.86	13.89	56	$n_{O(C(O))}$, $n_{O(OC)}$, π_{C1N1}
4	14.40	14.21	55	$n_{O(C(O))}$, $n_{O(OC)}$, π_{C1N1}
		14.91	54	σ_{C1N1}, σ_{C2N2}
5	15.18	15.17	53	σ_{C1N1}, σ_{C2N2}
6	15.71	15.73	52	n_F
7	16.11	16.28	51	n_F

[a]OVGF from geometries at the B3LYP/6- 311+G(d) level of approximation.

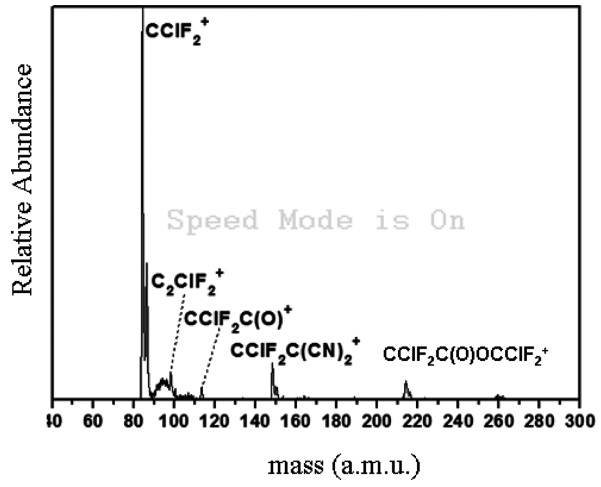

Figure 8. He(I) photoionization mass spectrum (PIMS) of $CClF_2C(O)OC(CN)_2CClF_2$.

(~ 240 cm^{-1}). For comparison, computed values of the most stable *gauche-syn-gauche* form are listed in Table 4.

The vertical ionization energies observed in the photoelectron spectrum of $CClF_2C(O)OC(CN)_2CClF_2$ agree with the calculated values of the OVGF method. The first band in the photoelectron spectrum, centered at 12.13 eV, can be attributed to the ionization process from the highest occupied molecular orbital (HOMO), which corresponds to carbonylic oxygen lone-pair electrons (n_O). This ionization energy was also reported at 12.00 eV for the monomeric species $CClF_2C(O)CN$ indicating the lack of influence of the vicinal orbitals in the dimeric species.[2]

The second and third ionization bands observed at 12.27 and 13.09 eV can be attributed to the process involving the chlorine lone pairs of the group $CClF_2C(O)$. Moreover, the calculation of these lone pairs in the group $CClF_2C(CN)_2$ is computed at 13.21 eV. Therefore, overlapped signals may be anticipated in this region. Following the trend listed in Table 4 the signal at 13.84 eV can be attributed to the another chlorine lone pair (n_{Cl}) of the group $CClF_2C(CN)_2$

The following ionization bands observed in the photoelectron spectrum are assigned as listed in the Table 4.

$CF_3C(O)OC(CN)_2CF_3$. The photoelectron spectrum of $CF_3C(O)OC(CN)_2CF_3$ is shown in the Figure 7, whereas Table 5 lists its experimental and calculated ionization energies and MO characters. The schematic representation of the 12 higher HOMOs is given in Figure S5 (Supporting Information).

dx.doi.org/10.1021/jp4127732 | J. Phys. Chem. A 2014, 118, 1721−1729

The first band in the photoelectron spectrum, centered at 12.43 eV, can be assigned to the ionization process from the highest occupied molecular orbital (HOMO), which also can be endorsed to carbonylic oxygen lone-pair electrons (n_O). This ionization energy was also reported at 12.13 eV for the dimeric species $CClF_2C(O)OC(CN)_2CClF_2$ and at 12.00 eV in $CClF_2C(O)CN$ supporting this assignment.[2]

The second ionization potential at 13.65 eV can be attributed to the lone pairs of the C−O−C oxygen with remarkable π bonding contributions from the vicinal CN groups. The third and fourth bands in the PES of $CF_3C(O)OC(CN)_2CF_3$ are linked with ionizations from π orbitals of the two CN groups. Table 5 lists also the remainder bands and their assignments.

Photoionization Mass Spectrum. *$CClF_2C(O)OC(CN)_2CClF_2$.* The ultraviolet photoionization mass spectrum (PIMS) of $CClF_2C(O)OC(CN)_2CClF_2$ was determined together with the photoelectron spectra and is shown in Figure 8. The PIMS confirms the identity of the sample. The spectrum of $CClF_2C(O)OC(CN)_2CClF_2$ shows peaks originated from the fragments $C^{35}ClF_2^+$ (85 a.m.u.), $C^{37}ClF_2^+$ (87 a.m.u.), $C_2ClF_2^+$ and $CClF_2C(O)^+$ (without isotopomeric resolution), $C^{35}ClF_2C(CN)_2^+$ (149 a.m.u.), $C^{37}ClF_2C(CN)_2^+$ (151 a.m.u.), $C^{35}ClF_2C(O)OC^{35}ClF_2^+$ (214 a.m.u.), and $C^{37/35}ClF_2C(O)OC^{35/37}ClF_2^+$ (216 a.m.u.) formed by the extrusion of a central $C(CN)_2$ and followed by subsequent rearrangement process.

$CF_3C(O)OC(CN)_2CF_3$. Figure 9 shows the photoionization mass spectrum corresponding to $CF_3C(O)OC(CN)_2CF_3$. The most intense signal at $m/Z = 69$ corresponds to the CF_3^+ ion in analogy with the behavior observed for the dimeric chlorinated species $CClF_2C(O)OC(CN)_2CClF_2$. Peaks at 97 and 133 a.m.u. can also be observed. In this compound and in comparison with $CClF_2C(O)OC(CN)_2CClF_2$ a higher stability of the heavier fragments becomes apparent as is the case of the fragment at 189 a.m.u. corresponding to $CF_3C(O)OC(CN)_2C^+$. For both compounds analyzed in this work, the observed fragments give reliability to the identity of the samples and to the PES.

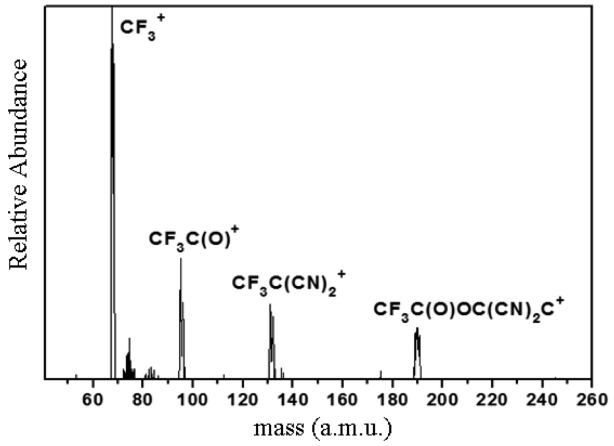

Figure 9. He(I) photoionization mass spectrum (PIMS) of $CF_3C(O)OC(CN)_2CF_3$.

CONCLUSIONS

The new dimer of $CClF_2C(O)CN$, $CClF_2C(O)OC(CN)_2CClF_2$, has been synthesized and characterized. Quantum chemical calculations compute a *gauche-syn-gauche* conformation for the most abundant form and the coexistence of other conformers in the gas phase at ambient temperature. In practice, however, only the two lowest energy *gauche-syn-gauche* and *gauche-syn-anti* rotamers were observed when the vapor was trapped in a solid Ar matrix. The study of the dimer of $CF_3C(O)CN$, $CF_3C(O)OC(CN)_2CF_3$, is also presented in this work for the sake of comparison. Only one *syn-syn-anti* conformation was observed for this compound. The influence of the electronegativity of the groups attached to the carbonyl group on the energy potential of these species becomes apparent from the comparison presented in Figure 10. With the exception of $CClF_2C(O)NCS$ with the lower potential energy due to the presence of S in its molecule, the remaining examples follow an electronegativity trend, including $CClF_2C(O)NCS$ if the ionization process initiated by the O lone pair, and not by the S lone pair, is formally taken into account. Thus, a higher electronegativity sum of the C═O substituents promotes a molecular energy stabilization and an increase in the corresponding ionization energies.

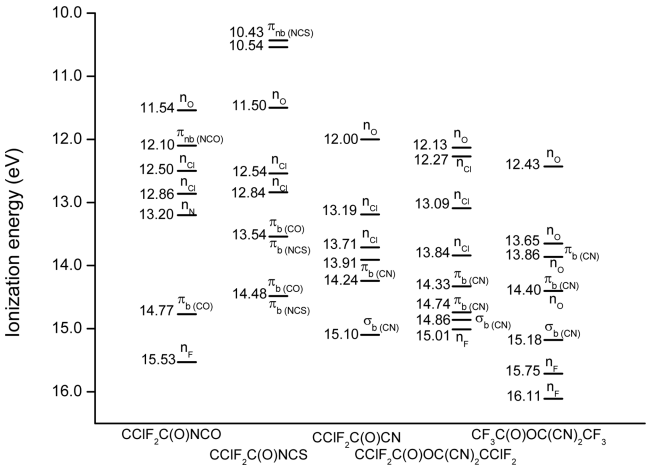

Figure 10. Ionization energy correlation diagram for $CF_3C(O)OC(CN)_2CF_3$, $CClF_2C(O)OC(CN)_2CClF_2$, and related species.

ASSOCIATED CONTENT

Supporting Information

^{19}F NMR and ^{13}C NMR of $CClF_2C(O)OC(CN)_2CClF_2$ and $CF_3C(O)OC(CN)_2CF_3$ at room temperature. UV−visible spectra of gaseous of $CClF_2C(O)OC(CN)_2CClF_2$ and $CF_3C(O)OC(CN)_2CF_3$ and its comparison with $CClF_2C(O)CN$. The first 12 HOMOs of both $CClF_2C(O)OC(CN)_2CClF_2$ and $CF_3C(O)OC(CN)_2CF_3$ computed with the approximation B3LYP/6-311+G(d). This information is available free of charge via the Internet at http://pubs.acs.org.

AUTHOR INFORMATION

Corresponding Author

*E-mail: carlosdv@quimica.unlp.edu.ar.

Notes

The authors declare no competing financial interest.

ACKNOWLEDGMENTS

The authors thank the Deutscher Akademischer Austauschdienst Germany (DAAD), Agencia Nacional de Promoción Científica y Técnica (ANPCYT), Consejo Nacional de Investigaciones Científicas y Técnicas (CONICET), Comisión de Investigaciones de la Provincia de Buenos Aires (CIC), Facultad de Ciencias Exactas and Universidad Nacional de La Plata (UNLP)

for financial support. L.A.R. gratefully acknowledges the DAAD, UNLP and Bergische Universität Wuppertal. C.O.D.V. acknowledges the DAAD, which generously sponsors the DAAD Regional Program of Chemistry for Argentina supporting Latin-American students to carry out Ph.D. research in La Plata. H.B. and H.W. acknowledge the support of the Deutsche Forschungsgemeinschaft. C.O.D.V. and R.M.R. acknowledge the support of the Chinese Academy of Sciences to work in the Institute of Chemistry of the Chinese Academy of Science in Beijing.

REFERENCES

(1) Ardis, A. E.; Averill, S. J.; Gilbert, H.; Miller, F. F.; Schmidt, R. F.; Stewart, F. D.; Trumbull, H. L. Vinylidene Cyanide. I. *J. Am. Chem. Soc.* **1950**, *72*, 1305−1307.

(2) Ramos, L. R.; Ulic, S. E.; Romano, R. M.; Tong, S.; Ge, M.; Berger, R. J.; Hayes, S. A.; Mitzel, N. W.; Beckers, H.; Willner, H.; et al. Chlorodifluoroacetyl Cyanide, $ClF_2CC(O)CN$: Synthesis, Structure, and Spectroscopic Characterization. *Inorg. Chem.* **2011**, *50*, 9650−9659.

(3) Tate, B. E.; Bartlett, P. D. The Dimerization of Acetyl Cyanide. *J. Am. Chem. Soc.* **1956**, *78*, 5575−5580.

(4) Lidy, W.; Sundermeyer, W. Darstellung und Eigenschaften Einiger Trifluoroacetyl-Pseudohalogenide. *Chem. Ber.* **1976**, *109*, 1491−1496.

(5) Mortimer, S. A.; Weeks, K. M. Time-Resolved RNA SHAPE Chemistry: Quantitative RNA Structure Analysis in One-Second Snapshots and at Single-Nucleotide Resolution. *Nature Protocol* **2009**, *4*, 1413−1421.

(6) Grohman, J. K.; Gorelick, R. J.; Lickwar, C. R.; Lieb, J. D.; Bower, B. D.; Znosko, B. M.; Weeks, K. M. A Guanosine-Centric Mechanism for RNA Chaperone Function. *Science* **2013**, *340*, 190−195.

(7) Gombler, W.; Willner, H. A Method for Opening and Resealing Glass Ampoules Several Times Under Sustained Vacuum. *J. Phys. E: Sci. Instrum.* **1987**, *20*, 1286−1288.

(8) Schnöckel, H. G.; Willner, H. *Infrared and Raman Spectroscopy, Methods, and Applications*; VCH: Weinheim, Germany, 1994; pp 297−299.

(9) Frisch, M. J.; Trucks, G. W.; Schlegel, H. B.; Scuseria, G. E.; Robb, M. A.; Cheeseman, J. R.; Montgomery Jr., J. A.; Vreven, T.; Kudin, K. N.; Burant, J. C. et al. *Gaussian 03*, revision B.04 ed.; Gaussian, Inc.: Pittsburgh, PA, 2003.

(10) Erben, M. F.; Boese, R.; Willner, H.; Della Védova, C. O. Chlorodifluorothioacetic Acid, $CF_2ClC(O)SH$: Synthesis, Characterization, X-ray Structure, and Conformational Properties. *Eur. J. Org. Chem.* **2007**, 4917−4926.

(11) Gómez Castaño, J. A.; Romano, R. M.; Beckers, H.; Willner, H.; Della Védova, C. O. Preparation and Properties of $HCF_2C(O)SeH$ and $ClCF_2C(O)SeH$. *Inorg. Chem.* **2012**, *51*, 2608−2615.

(12) Balfour, W. J.; Fourgere, S. G.; Klapstein, D. The Vibrational Spectrum of Cyanoformyl Fluoride. *Spectrochim. Acta, Part A* **1991**, *47*, 1127−1130.

(13) Ramos, L. A.; Ulic, S. E.; Romano, R. M.; Vishnevskiy, Y. V.; Berger, R. J. F.; Mitzel, N. W.; Beckers, H.; Willner, H.; Tong, S.; Ge, M.; et al. Chlorodifluoroacetyl Isocyanate, $ClF_2CC(O)NCO$: Preparation, Structural and Spectroscopic Studies. *J. Phys. Chem. A* **2012**, *116*, 11586−11595.

(14) Ramos, L. A.; Ulic, S. E.; Romano, R. M.; Vishnevskiy, Y. V.; Mitzel, N. W.; Beckers, H.; Willner, H.; Tong, S.; Ge, M.; Della Védova, C. O. Chlorodifluoroacetyl Isothiocyanate, $ClF_2CC(O)NCS$: Preparation, Structural and Spectroscopic Studies. *J. Phys. Chem. A* **2013**, *117*, 5597−5606.

(15) Ramos, L. A.; Zeng, X.; Ulic, S. E.; Beckers, H.; Willner, H.; Della Védova, C. O. Chlorodifluoroacetyl Azide, $ClF_2CC(O)N_3$: Preparation, Properties and Decomposition. *J. Org. Chem.* **2012**, *77*, 6456−6462.

(16) Barnes, A. J. In *Matrix Isolation Spectroscopy*; Barnes, A. J.; Orville-Thomas, W. J.; Müller, A.; Gaufrés, R., Eds.; NATO ASI, Series C; Reidel Publishing: Dordrecht, The Netherlands, 1981; Vol. *6*.

(17) Durig, J. R.; Guirgis, G. A.; Krutules, K. A. Raman and Infrared Spectra, Conformational Stability, Barriers to Internal Rotation, and Ab Initio Calculations of Trifluoroacetyl Isocyanate. *J. Mol. Struct.* **1994**, *328*, 55−75.

(18) Kagarise, R. E. Relation Between the Electronegativities of Adjacent Substitutents and the Stretching Frequency of the Carbonyl Group. *J. Am. Chem. Soc.* **1955**, *77* (5), 1373−1379.

(19) Yao, L.; Ge, M. F.; Wang, W.; Zeng, X.; Sun, Z.; Wang, D. Gas Phase Generation and Electronic Structure Investigation of Chlorosulfanyl Thiocyanate ClSSCN. *Inorg. Chem.* **2006**, *45*, 5971−5975.

(20) Zeng, X.; Ge, M. F.; Sun, Z.; Wang, D. Nitrosyl Isocyanate (ONNCO): Gas Phase Generation and a HeI Photoelectron Spectroscopy Study. *Inorg. Chem.* **2005**, *44*, 9283−9287.

(21) Zeng, X.; Liu, F.; Sun, Q.; Ge, M. F.; Zhang, J.; Ai, X.; Meng, L.; Zheng, S.; Wang, D. Reaction of AgN_3 with $SOCl_2$: Evidence for the Formation of Thionyl Azide $SO(N_3)_2$. *Inorg. Chem.* **2004**, *43*, 4799−4801.